JACS
JOURNAL OF THE AMERICAN CHEMICAL SOCIETY

ARTICLE

pubs.acs.org/JACS

High-Spin Cobalt(II) Ions in Square Planar Coordination: Structures and Magnetism of the Oxysulfides $Sr_2CoO_2Cu_2S_2$ and $Ba_2CoO_2Cu_2S_2$ and Their Solid Solution

Catherine F. Smura,[†] Dinah R. Parker,[†] Mohamed Zbiri,[‡] Mark R. Johnson,[‡] Zoltán A. Gál,[†] and Simon J. Clarke*[,†]

[†]Inorganic Chemistry Laboratory, Department of Chemistry, University of Oxford, South Parks Road, Oxford OX1 3QR, U.K.

[‡]Institut Max von Laue-Paul Langevin, 6 rue Jules Horowitz, BP 156, 38042 Grenoble Cedex 9, France

Supporting Information

ABSTRACT: The antiferromagnetic structures of the layered oxychalcogenides $(Sr_{1-x}Ba_x)_2CoO_2Cu_2S_2$ $(0 \le x \le 1)$ have been determined by powder neutron diffraction. In these compounds Co^{2+} is coordinated by four oxide ions in a square plane and two sulfide ions at the apexes of an extremely tetragonally elongated octahedron; the polyhedra share oxide vertexes. The magnetic reflections present in the diffraction patterns can in all cases be indexed using a $\sqrt{2}a \times \sqrt{2}a \times c$ expansion of the nuclear cell, and nearest-neighbor Co^{2+} moments couple antiferromagnetically within the CoO_2 planes. The ordered magnetic moment of Co^{2+} in $Sr_2CoO_2Cu_2S_2$ $(x = 0)$ is 3.8(1) μ_B at 5 K, consistent with high-spin Co^{2+} ions carrying three unpaired electrons and with an additional significant unquenched orbital component. Exposure of this compound to moist air is shown to result in copper deficiency and a decrease in the size of the ordered moment to about 2.5 μ_B; there is a strong correlation between the size of the long-range ordered moment and the occupancy of the Cu site. Both the tetragonal elongation of the CoO_4S_2 polyhedron and the ordered moment in $(Sr_{1-x}Ba_x)_2CoO_2Cu_2S_2$ increase with increasing Ba content, and in $Ba_2CoO_2Cu_2S_2$, which has Co^{2+} in an environment that is close to purely square planar, the ordered moment of 4.5(1) μ_B at 5 K is over 0.7 μ_B larger than that in $Sr_2CoO_2Cu_2S_2$, so the unquenched orbital component in this case is even larger than that observed in octahedral Co^{2+} systems such as CoO. The experimental observations of antiferromagnetic ground states and the changes in properties resulting from replacement of Sr by Ba are supported by *ab initio* calculations on $Sr_2CoO_2Cu_2S_2$ and $Ba_2CoO_2Cu_2S_2$. The large orbital moments in these systems apparently result from spin−orbit mixing of the unequally populated d_{xz}, d_{yz}, and d_{z^2} orbitals, which are reckoned to be almost degenerate when the CoO_4S_2 polyhedron reaches its maximum elongation. The magnitudes of the ordered moments in high-spin Co^{2+} oxide, oxychalcogenide, and oxyhalide systems are shown to correlate well with the tetragonal elongation of the coordination environment. The large orbital moments lead to an apparently magnetostrictive distortion of the crystal structures below the Neél temperature, with the symmetry lowered from tetragonal *I*4/*mmm* to orthorhombic *Immm* and the size of the distortion correlating well with the size of the long-range ordered moment for all compositions and for temperature-dependent data gathered on $Ba_2CoO_2Cu_2S_2$.

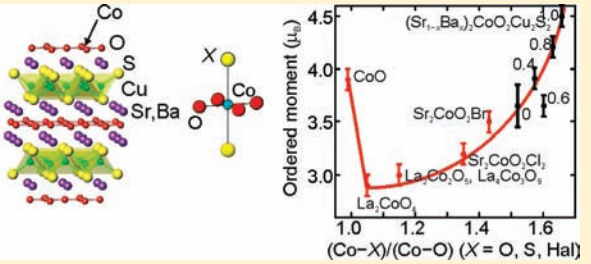

INTRODUCTION

Oxychalcogenides are a relatively under-investigated class of solid-state compounds compared with oxides and other solids containing only one type of anion. Due to the different sizes and coordination requirements of the oxide and the heavier chalcogenide anions, oxychalcogenides tend to adopt layered structures. In the oxysulfides $A_2MO_2Cu_2S_2$ (where A is an alkaline earth metal and M is a transition metal; compounds known for A = Sr, M = Mn,[1] Co,[2] Ni,[3] Cu,[3] and Zn,[1] and for A = Ba, M = Co,[2] which were first described, along with a series of related compounds, by Zhu and Hor and co-workers[1]), the more polarizable sulfide anion bonds to Cu^+ in $(Cu_2S_2)^{2-}$ antifluorite-type layers, and the less polarizable oxide anion bonds to the divalent M^{2+} in square planar $(MO_2)^{2-}$ layers which are two-dimensional fragments of the perovskite structure. The two layer types stack alternately with A^{2+} cations in between. The transition metal cation M is in the center of a highly tetragonally distorted MO_4S_2 octahedron. Oxychalcogenides with these layered structures provide a counterpoint to important perovskite-related oxide phases, such as the three-dimensional cubic perovskites $AMO_{3-\delta}$ and the layered Ruddlesden−Popper $(A_{n+1}M_nO_{3n+1})$ phases. It is well-established[4] that the chalcogenide layers present in the oxysulfides can readily accept holes in

Received: November 2, 2010
Published: February 8, 2011

the antibonding states at the top of a valence band that is composed of well-mixed Cu 3d/S 4p orbitals and that these holes are very mobile. So the band gap insulator $Sr_2ZnO_2Cu_2S_2$ may be doped to produce a p-type metal, $Na_xSr_{2-x}ZnO_2Cu_2S_2$, with $x \approx 0.1$.[5] When the valence band is not doped with holes and the metal M in the oxide layer is a mid-to-late transition metal, the compounds are semiconducting,[2,6] suggesting that the oxide layer behaves as a Mott−Hubbard insulator. The interactions between the two electronically very different layers is via weak bonding interactions between M and S, which may in principle be tuned by the size of the A cation. It is expected that investigation of compounds with this structure type could lead to unusual magnetic and electronic behaviors complementary to those of the better-studied oxides. The oxysulfides, by virtue of containing anions of less electronegative Group 16 elements, also tend to exhibit lower oxidation states for the transition metals than are found in perovskite-type oxides. For example, the homologous series of compounds $Sr_2MnO_2Cu_{2m-\delta}S_{m+1}$ (m = 1, 2, 3; δ = 0.5) that we have described[6] contains Mn in a mean oxidation state of +2.5 instead of the oxidation states between +3 and +4 that are more normally encountered in manganite perovskites. Furthermore, these compounds offer high-symmetry structures with transition metal ions in strictly planar oxide layers, irrespective of the nature of the alkaline earth cation or the chalcogenide anion, and may be good model compounds that will contribute to the development of theories of low-dimensional solids. Related oxychalcogenides include compounds containing planar M_2O layers with M two-coordinate by oxide and four-coordinate by chalcogenide ions, such as $La_2Fe_2Se_2O_3$[7] and the recently reported $La_2Co_2Se_2O_3$.[8,9]

The synthesis and characterization of the first layered cobalt oxysulfides, $A_2CoO_2Cu_2S_2$ (A = Sr, Ba), containing square planar CoO_2 layers, were reported by Zhu et al.[2] It was reported that the compound with A = Sr could also support a small copper deficiency, and a pure phase with composition $Sr_2CoO_2Cu_{1.75}S_2$ was described. All subsequent property measurements on $Sr_2CoO_2Cu_2S_2$ have been made on samples synthesized with what we assume, in the absence of statements to the contrary, to be full Cu site occupancy and handled at least partly in ambient air.[2,10−12] Magnetic susceptibility measurements on $Sr_2CoO_2Cu_2S_2$ and $Ba_2CoO_2Cu_2S_2$ show broad maxima at about 220 K[2,10] and about 230 K,[2] respectively, and this, together with the observation in $Sr_2CoO_2Cu_2S_2$ of magnetic Bragg peaks in neutron powder diffraction patterns obtained below 200 K,[2] suggests low-dimensional antiferromagnetic ordering of the Co^{2+} ions. The magnetic structures of $Sr_2CoO_2Cu_2S_2$ and $Ba_2CoO_2Cu_2S_2$ have not been reported, nor have the magnitudes of the ordered moments of the Co^{2+} sublattice. $Sr_2CoO_2Cu_2S_2$ has been found to show a divergence in field-cooled (FC) and zero-field-cooled (ZFC) magnetic susceptibilities below 80 K[2,10] that is not observed in the Ba analogue. This apparent spin-glass-type behavior in $Sr_2CoO_2Cu_2S_2$ appears to be nonconventional because the rate of decay of the magnetization is slower at 10 and 75 K than at an intermediate temperature (45 K) and the time dependence of the magnetization cannot be fit to a stretched exponential form.[13] $Sr_2CoO_2Cu_2S_2$ was also reported to show semiconducting behavior, while the resistivity of the Ba analogue is 10^4 times higher.[2] Subsequent investigations of the dielectric response and the transport properties of sintered powders of $Sr_2CoO_2Cu_2S_2$[12] seem to suggest a possible spin-carrier phase separation below T_N: electron transfer from the S 3p-based states at the top of the valence band onto Co results in mobile holes in the chalcogenide layer and an insulator-to-metal transition on cooling. However, there is no clear consensus in the literature as to the nature of the behavior of $Sr_2CoO_2Cu_2S_2$. This paper shows that $Sr_2CoO_2Cu_2S_2$ is subject to aerial oxidation, with important implications for the composition and magnetic properties, which suggest that some re-evaluation of some of the reported properties of this compound may be required. Here we describe the crystal and magnetic structures of the members of the solid solution $Sr_{2-x}Ba_xCoO_2Cu_2S_2$ ($0 \le x \le 2$), which offer very unusual examples of high-spin Co^{2+} ions in a ligand field that, especially in the Ba-rich members, is very close to being purely square planar because the CoO_4S_2 polyhedron is extremely tetragonally distorted with very long Co−S distances. In all these compounds, the Co^{2+} ion carries an unquenched orbital contribution to its magnetic moment. We correlate the trends in the size of the ordered magnetic moment and the details of the low-temperature structures with the increasing tetragonal elongation of the CoO_4S_2 polyhedron as Sr^{2+} is replaced by the larger Ba^{2+} cation, and we compare this behavior with that reported for other magnetically concentrated Co^{2+} systems. Our experimental results are supported by *ab initio* computational investigations of the end member compounds that enable electronic and magnetic properties to be correlated with the crystal structures.

EXPERIMENTAL SECTION

Synthesis. In all syntheses of oxysulfides, the reagents were cold pressed into pellets and contained in alumina crucibles inside sealed, predried evacuated silica tubes. Due to the air sensitivity of many of the reagents and the products, manipulations of the solids prior to synthesis were always performed in a Glovebox Technology Ltd. argon-filled glovebox with an O_2 and H_2O content of less than 1 ppm. In general the products were also handled under argon, but see below. $(Sr_{1-x}Ba_x)_2CoO_2Cu_2S_2$ ($0 \le x \le 1$) were generally synthesized by reacting together ($(1-x)$SrS + xBaS), CuO (Aldrich, 99.99%), and Co (Aldrich, 99.995%) in the molar ratio 2:2:1 at a temperature of 850 °C (x = 2) or 825 °C (x < 2) for 48 h. In some syntheses of $Sr_2CoO_2Cu_{2-\delta}S_2$ samples, copper deficiency was introduced by using Co_3O_4 as a fourth reactant (i.e., SrS, CuO, Co_3O_4 (Alfa, 99.9985%) and Co in the molar ratio 2:1.85:0.0375:0.8875 for the composition $Sr_2CoO_2Cu_{1.85}S_2$). In later syntheses of $Sr_2CoO_2Cu_2S_2$ samples, the reactants were SrO, Co, Cu (Alfa, 99.99%) and S (Alfa, 99.999%) in a 2:1:2:2 ratio, and in these cases the sealed ampules were heated to 400 °C for 16 h to ensure reaction of sulfur with the elemental metals prior to heating to the synthesis temperature of 825 °C at 1 °C min^{-1} and maintaining this temperature for 32 h. SrO was made by decomposing $SrCO_3$ (Alfa, 99.994%) at 900 °C under vacuum, with a final firing at 1100 °C to ensure complete decomposition. BaS and SrS were made by heating $BaCO_3$ (Alfa, 99.95%) and $SrCO_3$ at 800 °C in a flow of CS_2 (Aldrich, 99.5%) vapor, transported by bubbling argon through the liquid, for two periods of 5 h with intermediate grinding.

Caution! CS_2 is highly toxic and highly flammable. The gas emerging from the flow system was passed through hydroxide bleach to destroy excess CS_2, and the flow system was purged with pure argon after the apparatus had cooled to room temperature; the entire apparatus was contained in a fume hood.

X-ray Powder Diffraction (XRPD). XRPD was used to assess the phase purity of reactants and products prepared as described above. Measurements were made using a PANalytical X'Pert PRO diffractometer operating in Bragg−Brentano geometry with monochromatic Cu Kα_1 radiation and a multiangle X'Celerator detector. High-resolution measurements on $Sr_2CoO_2Cu_2S_2$ samples were performed on Station ID31 at the ESRF, Grenoble, using X-rays with Si-calibrated

wavelengths of 0.4−0.45 Å and with the samples contained in 0.7 mm diameter glass capillary tubes. The capillaries were filled with helium exchange gas to ensure good thermal contact between the powder and the He flow cryostat and to avoid heating of the sample by the intense X-ray beam. In early experiments on ID31, we discovered that, when the capillaries were sealed under argon, below about 50 K the peak shapes broadened and became highly asymmetric and the lattice parameters showed an anomalous expansion, reaching values as large as or even exceeding their room-temperature values (see Supporting Information, Figure S9). This behavior we attribute to beam-heating of the sample when the exchange gas has condensed.

Neutron Powder Diffraction (NPD). Time-of-flight (ToF) NPD data were collected at the ISIS Facility, Rutherford Appleton Laboratory, UK, using the medium-resolution diffractometer POLARIS, the high-resolution powder diffractometer HRPD, and the diffractometer OSIRIS, which is optimized for high-resolution studies at long *d*-spacings. On POLARIS, samples of 2−5 g mass were sealed inside cylindrical thin-walled vanadium cans using indium gaskets and measured between 2 and 298 K in the *d*-spacing range 0.4 < d < 8 Å by means of three banks of detectors located at scattering angles, 2θ, of 35° (^{3}He tube detector), 90° (ZnS scintillator), and 145° (^{3}He tube detector; highest resolution bank, $\Delta d/d = 5 \times 10^{-3}$). Total integrated proton currents at the production target were typically 500−1000 μA·h·g for these measurements. On HRPD, a 10 g sample of $Ba_2CoO_2Cu_2S_2$ (CFS044) was contained in an aluminum "slab" can with vanadium windows, and a thin gadolinium foil was used to mask the aluminum. Measurements were carried out at 5−10 K intervals between 4 and 250 K for an integrated proton current of 17 μA·h (30 min runs). Four-gram samples of samples of $Sr_{2-x}Ba_xCoO_2Cu_2S_2$ with x = 0.6, 0.7, 0.8, and 0.9 were also measured at 4 K on HRPD, for a total integrated proton current at the production target of 75 μA·h. Neutrons were measured using three detector banks at 168° (ZnS scintillator; highest resolution bank, $\Delta d/d = 4 \times 10^{-4}$), 90° (ZnS scintillator), and 35° (^{3}He tubes). On OSIRIS, data were collected on 4 g samples of $Sr_{2-x}Ba_xCoO_2Cu_2S_2$ with x = 0, 0.4, 0.7, and 0.8 over the *d*-spacing range 0.5−8 Å in six overlapping segments using a single detector bank at 160° (^{3}He tubes; $\Delta d/d \approx 4 \times 10^{-3}$), for an integrated proton current of 40 μA·h.

Data were also collected using monochromatic radiation between 5 K and room temperature on 4 g samples of $Ba_2CoO_2Cu_2S_2$ and $Sr_2CoO_2Cu_2S_2$ using the D2B diffractometer at the Institut Laue-Langevin (ILL), Grenoble. Measurements were made using neutrons of wavelength 1.59 Å selected by diffraction from the (335) planes of a 28-crystal Ge monochromator. Patterns were collected over about 4 h using an array of 128 high-pressure ^{3}He detectors with a step size of 0.05° in 2θ. Further measurements of $Sr_2CoO_2Cu_2S_2$ samples were made on D1A at ILL using 1.9 Å neutrons selected using the (115) planes of a 30-crystal Ge monochromator. All structural refinements against PND data were carried out using the Rietveld profile refinement suite, GSAS.[14] Refinement against data collected on POLARIS was carried out using all three detector banks simultaneously, and on HRPD the 90° and 168° banks were used. The magnetic form factor for Co^{2+} used in the refinements was obtained from standard tables.[15]

X-ray Single Crystal Diffraction. Measurements were performed a single crystal of $Ba_2CoO_2Cu_2S_2$ with a Nonius Kappa CCD diffractometer using Mo Kα (λ = 0.71073 Å) incident radiation. The crystal was mounted on a nylon loop using paratone oil, and measurements were made at room temperature and at 110 K using an Oxford Instruments cooling system integral to the diffractometer. Data reduction was performed using the DENZO-SMN software package.[16] Structure solution (using Direct Methods) and full matrix least-squares refinement via the WinGX[17] suite were carried out using SHELXS97 and SHELXL97, respectively.[18] The data were corrected for Lorentz-polarization, and a face-indexed numerical absorption correction was applied through the PLATON interface.[19]

Magnetic Susceptibility Measurements. Measurements were carried out using either a Quantum Design MPMS5 or MPMS-XL SQUID magnetometer in the temperature range 5−330 K. Measurements were made on warming in a field of 0.01 or 0.1 T, first after cooling in zero field (ZFC) and then again after cooling in the measuring field (FC). The measured moment of $Ba_2CoO_2Cu_2S_2$ at room temperature did not show a linear relationship with the applied field in the low-field region, presumably due to the presence of minuscule amounts of an unidentified ferromagnetic impurity. Measurement of the sample's true bulk susceptibility was made by recording the moment as a function of temperature in fields of 3 and 4 T (i.e., in the region in which the ferromagnetic impurity had saturated), allowing calculation of the moment at an "effective" field of 1 T.

Computational Investigations. Calculations were carried out using the projector augmented wave (PAW) formalism[20] of the Kohn−Sham formulation of the spin-polarized density functional theory (KSDFT)[21,22] at the generalized gradient approximation (GGA) level, implemented in the Vienna Ab-initio Simulation Package (VASP).[23,24] The GGA was formulated by the Perdew−Burke−Ernzerhof (PBE)[25,26] density functional. Electron correlation plays a predominant role when magnetic interactions in transition-metal-containing materials are studied. Indeed, the strongly correlated character of the electrons in the open-shell 3d levels of Co^{2+} should be described accurately, and the self-interaction error related to the density functional description of the magnetic unpaired Co 3d electrons should be corrected. In this context, the Hubbard correction to the KSDFT has been considered employing the Dudarev approach.[27] In the latter formalism, the term $U_{eff} = U - J$, representing the difference between the on-site (U) and intersite (J) interactions, is added as a penalty functional to the KSDFT Hamiltonian. Thus, J was kept fixed at 0 eV, whereas different values were tested for the U parameter. All results were obtained using the experimental magnetic structures and adopting a fixed spin configuration corresponding to that observed. Further, non-collinear magnetic calculations considering the additional spin−orbit Hamiltonian were performed. The effect of spin−orbit coupling (SOC) was investigated by adopting different easy-axis orientations (in-plane and axial) to evaluate the dependence of the orbital magnetic moment contribution and the magnetic anisotropy.

RESULTS AND DISCUSSION

Composition and Room-Temperature Crystal Structure of $Sr_2CoO_2Cu_2S_2$. The initial report of $Sr_2CoO_2Cu_2S_2$ suggested that copper-deficient samples were possible and the phase width of $Sr_2CoO_2Cu_{2-\delta}S_2$ apparently covered the range $0 \le \delta \le 0.25$.[2] No air sensitivity was reported. We carried out a number of preliminary synthetic investigations in which the samples were handled in ambient air after the synthesis was complete. When samples of stoichiometric composition were prepared from the reaction between SrS, Co, and CuO, we discovered that elemental copper often precipitated out of the reaction, appearing on the surface of the pellets, suggesting the existence of copper-deficient phases as originally reported.[2] A powder neutron diffraction investigation on POLARIS of such a sample, which, apart from the existence of elemental copper, appeared very close to single phase by laboratory XRPD, revealed a refined value of the Cu-site occupancy of 0.961(2) at room temperature and 0.955(2) at 2 K. These two independent measurements agreed well at the two temperatures, showing that the wide *d*-spacing range on POLARIS minimizes correlation of the fractional site occupancy with the displacement parameters and sample absorption. An actual stoichiometry of $Sr_2CoO_2Cu_{1.91(1)}S_2$ for the oxysulfide phase was thus concluded from these results because

it seemed consistent with both the amount of elemental Cu in the sample and with the amount of Cu in the main phase. This led to attempts to prepare a range of single-phase samples with a copper deficiency.[28] In the course of these attempts, we discovered that the samples derived from copper-deficient mixtures of reagents persistently contained impurity phases (SrS and other unidentified impurities) that could not be eliminated by further grinding and heating cycles. We also discovered that samples of $Sr_2CoO_2Cu_2S_2$ were rather unobtrusively air-sensitive: although cursory inspection of laboratory X-ray diffractograms revealed no obvious degradation of samples over time (i.e., no new Bragg peaks were evident in the powder diffractograms), more detailed measurements revealed that there was a significant decrease (by 0.2−0.5%) in the unit cell volume on prolonged air exposure (over days and weeks). This also resulted in changes in the magnetic susceptibility, which we discuss further below. Once the air sensitivity was taken into account, NPD investigations of two samples synthesized with a composition $Sr_2CoO_2Cu_{1.85}S_2$ and never exposed to air (samples CFS127C and CFS130B) showed refined fractional occupancies of copper of at least 98−99%—i.e., much closer to stoichiometric $Sr_2CoO_2Cu_2S_2$ than intended (Supporting Information, Table S1).

We carried out a new series of experiments in order to (i) investigate the effect of air exposure on the magnetic properties and on the composition and structure, (ii) investigate the possible effect of the cooling rate from the synthesis temperature, and (iii) obtain reliable data on the low-temperature magnetic properties of $Sr_2CoO_2Cu_2S_2$. Two samples of stoichiometric material (i.e., the composition of the reactant mixture was $Sr_2CoO_2Cu_2S_2$) were prepared from the reactants SrO, Co, Cu, and S using two slightly different thermal treatments. One sample (DRP051) was cooled slowly from the synthesis temperature of 825 at 0.5 °C min^{-1}, and the other (DRP053) was cooled rapidly by quenching the sealed silica tube from 825 °C into iced water. Laboratory XRPD measurements of these samples revealed extremely small amounts of elemental Cu but no other obvious impurity phases. These two samples were each split into two portions. The first portion of each sample was stored in an argon-filled glovebox, while the second portion of each sample was exposed for about 16 h to a flow of oxygen that was bubbled through water upstream of the sample, in order to simulate rapidly the exposure of the sample to moist air. The resulting four samples were each investigated using NPD measurements. The two portions of the quenched sample (DRP053) were measured at room temperature on the POLARIS diffractometer at the ISIS facility, where the high Q-range is optimal for determining structural parameters and compositions. The two portions of this quenched sample were also measured at 5 K on the D2B diffractometer at ILL and at a series of temperatures using OSIRIS at ISIS, principally in order to probe the long-range magnetic ordering. The two portions of the slow-cooled sample (DRP051) were also measured on D2B at 5 K and at temperatures from 10 to 290 K on the high-resolution powder diffractometer ID31 at ESRF to probe changes in structure at low temperatures, which we discuss further below.

Refinement against the room-temperature data on the two portions of the quenched sample DRP053 collected on POLARIS (Figure 1) produced the results summarized in Table 1 and the structural model shown in Figure 4 (below). The sample that had received no air exposure was very close to stoichiometric in copper, with a refined composition of $Sr_2CoO_2Cu_{1.980(2)}S_2$. The neutron diffractogram contained very weak Bragg peaks due

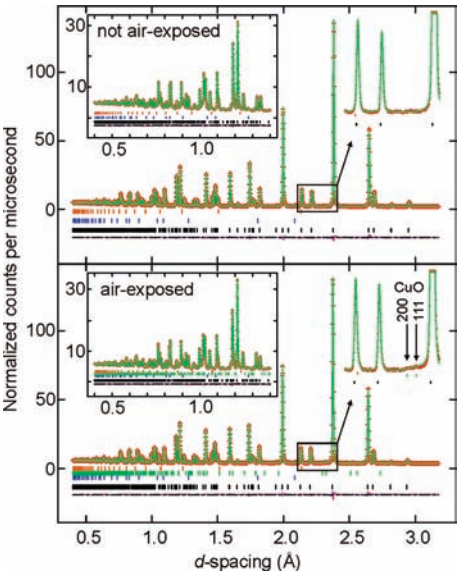

Figure 1. Rietveld refinements against POLARIS data for two portions of a single sample of $Sr_2CoO_2Cu_2S_2$ (quenched, DRP053). One portion had been carefully sequestered from air (upper refinement), and the other had received exposure to a flow of moist O_2 as described in the text (lower refinement). The insets show the low d-spacing regions and the appearance of broad reflections corresponding to the most intense reflections from the CuO that forms on exposure to moist O_2.

to elemental copper, and refinement of the phase fraction of elemental copper in the sample produced a value of 1.6(1) mol %, accounting, within the experimental uncertainty, for the remaining copper used in the synthesis but unaccounted for in the main phase. The second portion of this sample, which had received exposure to moist oxygen, had a unit cell volume 0.8% smaller than that of the unexposed portion of the same sample, and refinement of the fractional site occupancy of copper produced a refined composition of $Sr_2CoO_2Cu_{1.890(2)}S_2$, suggesting that 5% of the Cu present in the sample is lost through exposure to "moist air" in the form of a flow of H_2O-laden O_2. Note that the refined displacement parameters for Cu and the other atoms in the two portions of the sample are similar (Table 1), suggesting that the decrease in refined Cu content is real and not merely a consequence of parameter correlations in the refinement. Close examination of the NPD pattern of the portion of DRP053 that had been exposed to moist O_2 revealed no change in the phase fraction of elemental copper, but very broad additional scattering was evident, which was consistent with the formation of poorly crystalline CuO (Figure 1). Refinement of the phase fraction of CuO produced a mole fraction of 4.8(2)%, suggesting that on air exposure the oxysulfide sample is oxidized: copper ions are removed from the structure and form the oxide. We have previously shown that this oxidative deintercalation of copper on air exposure with the formation of poorly crystalline CuO occurs to a larger extent (∼13%) in stoichiometric samples of CeCuOS that have similar copper sulfide layers and contain the oxidizable Ce^{3+} cation.[29] The results obtained on the same two portions of this quenched sample DRP053 from the D2B diffractometer were quantitatively consistent with the results obtained from POLARIS and are summarized in Table S1 in the Supporting Information. The two portions of the slow-cooled sample (DRP051) analyzed on D2B (Table S1) showed behavior qualitatively similar to those of

Table 1. Rietveld Refinement Results against NPD Data for $Sr_2CoO_2Cu_{2-\delta}S_2$

radiation	neutron, ToF	
instrument	POLARIS	
T/K	298(2)	
space group	$I4/mmm$	
sample	DRP053 (quenched), unexposed portion	DRP053, air-exposed portion
a/Å	3.99129(2)	3.98354(2)
c/Å	17.71555(9)	17.6458(1)
V/Å^3	282.216(2)	280.014(2)
no. of variables	87	94
R_{wp}	0.0144	0.0116
R_{F^2}	0.0294	0.0272
χ^2	3.33	2.80
Sr z[a]	0.40767(1)	0.40646(1)
S z[a]	0.17119(3)	0.17072(3)
F(Cu)[b]	0.990(1)	0.945(1)
Sr $U_{eq} \times 10^2$ (Å^2)	0.71(1)	0.75(1)
Co $U_{eq} \times 10^2$ (Å^2)	0.91(2)	0.96(2)
Cu $U_{eq} \times 10^2$ (Å^2)	1.73(1)	1.76(1)
S $U_{eq} \times 10^2$ (Å^2)	0.81(1)	0.84(1)
O $U_{eq} \times 10^2$ (Å^2)	0.76(1)	0.80(1)
Co−O [4][c] (Å)	1.99565(1)	1.99177(1)
Co−S [2] (Å)	3.0327(5)	3.0126(5)
Sr−O [4] (Å)	2.5803(2)	2.5868(2)
Sr−S [4] (Å)	3.1491(3)	3.1288(3)
Cu−S [4] (Å)	2.4356(3)	2.4339(3)
S−Cu−S [2] (°)	110.04(2)	109.84(2)
S−Cu−S [4] (°)	109.19(1)	109.29(1)

[a] Co, 2a(0,0,0); O, 4c(0.5,0,0); Cu, 4d(0.5,0,0.25); Sr, 4e(0,0,z); S, 4e(0,0,z). Z = 2. [b] Site occupancy factor of Cu. [c] Numbers in square brackets indicate the multiplicity of each bond or angle.

DRP053. There is no significant difference in compositions of the portions of the samples that had received no exposure to air which could have arisen from the different thermal treatments during synthesis (i.e., the compositions appear to be unaffected by the rate of cooling from the synthesis temperature). On exposure to moist O_2, DRP051 underwent a decrease in cell volume of 0.5% and a decrease in Cu content of 3.5% ($Sr_2CoO_2Cu_{1.92(2)}S_2$), i.e., less than the corresponding values of 0.8% and 5% on oxidation of DRP053. These results reveal a good correlation with unit cell volume and Cu content. Using the high resolution of ID31 at ESRF, comparison at 290 K of the two portions of sample DRP051 (Figure 2) shows that air exposure results in asymmetric peak broadening, with full widths at half-maximum (fwhm) of all classes of reflection increasing by a factor of about 1.7. This is qualitatively similar to the behavior in CeCuOS on air exposure[29] and might arise from changes in particle size or particle strain or from inhomogeneity in the distribution of Cu in the sample. In summary, our synthetic and neutron diffraction investigations to probe the composition show that samples of nominal composition $Sr_2CoO_2Cu_2S_2$ appear to be intrinsically slightly copper deficient by about 1%. A much larger copper deficiency of about 5% is introduced by the oxidative de-intercalation of Cu in moist oxygen (or moist air) to produce CuO. The results of these experiments, in which pristine samples are exposed to H_2O-laden O_2 simulating moist

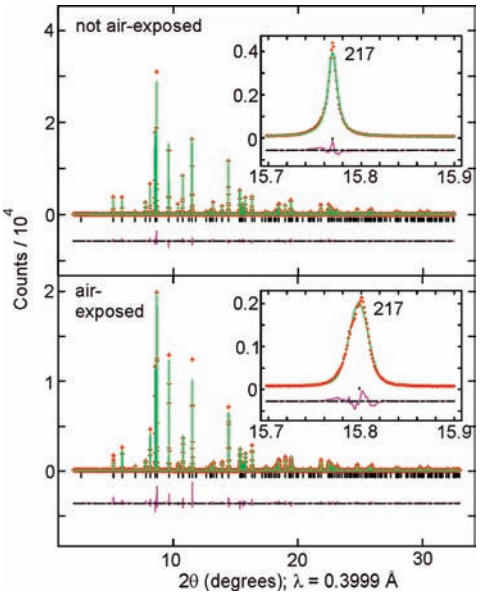

Figure 2. Rietveld refinements against ID31 data for two portions of a single sample of $Sr_2CoO_2Cu_2S_2$ (slow-cooled, DRP051). One had been carefully sequestered from air (upper), and the other had received exposure to a flow of moist O_2 as described in the text (lower). The insets show the effect of air exposure on the representative (217) reflection, which broadens significantly and moves to a shorter d-spacing as the unit cell contracts.

air, show that the unit cell volume can be used as a proxy for the Cu content. Comparison of portions of both sample DRP051 (synthesized as $Sr_2CoO_2Cu_2S_2$) and sample CFS126B (synthesized as $Sr_2CoO_2Cu_{1.85}S_2$) that had received no air exposure at 250 K on ID31 revealed lattice parameters of a = 3.98955(1) Å and c = 17.67726(7) Å for DRP051 and a = 3.98942(2) and c = 17.67198(9) Å for CFS126B, giving a difference in cell volumes of just 0.04%, consistent with the refined Cu occupancies of 0.985(7) (DRP051, D2B data) and 0.976(6) (CFS126B, D1A data), which are equal within the experimental uncertainty (see Supporting Information, Table S1 and Figure S1). Indeed, all our attempts to intentionally synthesize Cu-deficient materials at high temperatures led to the formation of oxysulfide phases that are very close to fully stoichiometric in copper with accompanying impurity phases. Significant copper deficiency is achieved only through low-temperature oxidative de-intercalation, which we have achieved here using moist O_2. Exposure of the sample CFS126B (prepared with nominal composition $Sr_2CoO_2Cu_{1.85}S_2$) to ambient laboratory air resulted in a decrease in the cell volume of 0.2%. Heating of this exposed sample under vacuum at 250 °C for 36 h led to an increase in the unit cell volume by 0.1%.[28] We presume that this indicates partial recovery of the stoichiometric material using low-temperature annealing, and this is supported by the magnetic susceptibility data described below, but we have not examined this behavior in further detail.

Consider the structural changes that occur on oxidative loss of copper from the structure of $Sr_2CoO_2Cu_2S_2$. Table 1 lists the important bond lengths and angles obtained from refinement against room-temperature POLARIS data on the two portions of sample DRP053 (quenched from the synthesis temperature). In the unexposed portion of this sample of $Sr_2CoO_2Cu_2S_2$, the Cu−S bond length of 2.4356(3) Å is similar to the values of

dx.doi.org/10.1021/ja109553u | J. Am. Chem. Soc. 2011, 133, 2691–2705

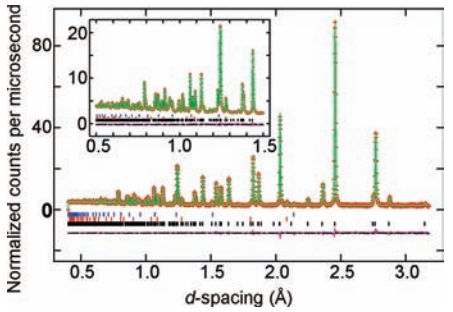

Figure 3. Rietveld refinements against POLARIS data for $Ba_2CoO_2Cu_2S_2$ (sample CFS028) at room temperature. The inset shows the low *d*-spacing region.

2.4410(9) and 2.4369 Å in the band insulators $Sr_2ZnO_2Cu_2S_2$[1] and LaCuOS,[30] respectively, with similar CuS layers and which must have filled Cu 3d/S 3p valence bands. In contrast, the value of the Cu−S distance in $TlCu_2S_2$,[31] which has one hole per formula unit in the Cu 3d/S 3p valence band, is 1.7% shorter (2.3943 Å) than in the insulating compounds because the depleted states at the top of the Cu 3d/S 3p band are antibonding.[4] In $Sr_2CoO_2Cu_2S_2$, loss of 5% of the Cu from the structure on air exposure generates 0.1 hole per formula unit, and the Cu−S distance contracts on oxidation from 2.4356(3) to 2.4339(3) Å. While these distances could be considered similar at the 3σ level, the change is only about half what would be expected if solely the Cu 3d/S 3p antibonding states are depleted on oxidation of $Sr_2CoO_2Cu_2S_2$ and if a linear decrease in Cu−S bond length with the number of holes per formula unit is assumed. The decreases in the Co−O and Co−S distances of 0.2% and 0.7%, respectively, are consistent with slight Co oxidation. Comparative bond valence sum calculations using literature parameters (for Co−O)[32] and estimated parameters (for Co−S)[33] suggest a 0.03 increase in Co oxidation state—i.e., about half what would be expected if solely Co^{2+} were oxidized. The changes in Cu−S, Co−O, and Co−S bond lengths are therefore consistent with partial oxidation of both Cu 3d/S 3p and Co 3d states. Removal of Cu, with no corresponding decrease in the Cu−S distance, would be expected to lead to underbonding of the sulfide ions, and it is observed that the Sr−S distance decreases significantly by 0.65% in order to maintain the bond valence of the sulfide ion. The Sr−O distance increases accordingly by 0.25%. The observation that the bonds to sulfide change most significantly is consistent with the loss of Cu^+, and this is in line with the results on CeCuOS.[29]

Composition and Room-Temperature Crystal Structure of $(Sr_{1-x}Ba_x)_2CoO_2Cu_2S_2$ ($0 \le x \le 1$). While $Sr_2CoO_2Cu_2S_2$ is rather unobtrusively air-sensitive, $Ba_2CoO_2Cu_2S_2$ is very obviously air-sensitive, decomposing readily in air to produce products that we did not attempt to analyze. The samples were kept in an inert atmosphere. The structure of $Ba_2CoO_2Cu_2S_2$, refined without incident from room-temperature XRSCD data, producing a refined composition of $Ba_2CoO_2Cu_{1.95(1)}S_2$. Independent refinement of the copper site occupancy factor and the phase fraction of excess elemental copper using POLARIS NPD data (Figure 3) also produced a composition of $Ba_2CoO_2Cu_{1.95(1)S2}$. NPD data from HRPD and D2B collected on two further samples suggested compositions of $Ba_2CoO_2Cu_{1.98(2)}S_2$ and $Ba_2CoO_2Cu_{1.98(1)}S_2$, respectively (Supporting Information, Table S2). The analysis suggests that, similar to the case of $Sr_2CoO_2Cu_2S_2$, there is a small intrinsic 1−2% copper deficiency

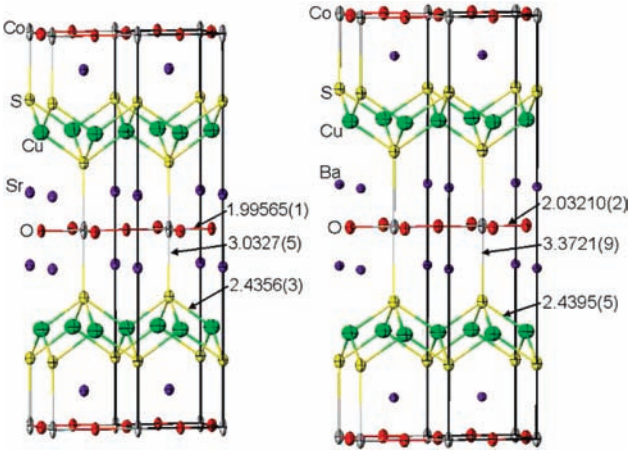

Figure 4. Structures of $Sr_2CoO_2Cu_2S_2$ (left) and $Ba_2CoO_2Cu_2S_2$ (right) obtained from refinement against POLARIS NPD data at room temperature and shown on the same scale. 95% anisotropic displacement ellipsoids are shown, and selected bond lengths are given in Å. Note the increase of almost 11% in the Co−S distance on substituting Sr by Ba. Further structural parameters are given in Table 2.

in these systems, and we cannot rule out a small phase width. The refinement results for the NPD and SXRD data and selected bond lengths are given in Table 2. The refined structures of $Sr_2CoO_2Cu_2S_2$ and $Ba_2CoO_2Cu_2S_2$ at room temperature are compared in Figure 4.

Analysis of POLARIS NPD data (Supporting Information, Figures S2 and S3, and Table 2) of the compounds $(Sr_{1-x}Ba_x)_2CoO_2Cu_2S_2$, synthesized assuming full occupancy of the tetrahedral sites in the sulfide layer by copper ions, revealed small amounts of elemental copper as the only obvious impurity phase in the NPD patterns. Analysis of the weight fraction of elemental copper suggested Cu deficiencies of 1−2%—similar to the values in the end members. Free refinement of the copper site occupancies for the phases containing both Sr and Ba systematically tended to produce values exceeding unity by 1−2%, presumably reflecting the effect of correlations with the displacement parameters, which are also systematically larger in these materials than in the end members of the solid solution (Tables 1 and 2). We have not investigated the possibility of variable copper deficiency in any of the Ba-containing compounds. In conclusion: across the entire solid solution, samples prepared using stoichiometric mixtures of reagents appear to be very slightly deficient in copper, but the deficiency is in the range 0−2%.

Structural Trends. The trends in lattice parameters and bond lengths for the series $(Sr_{1-x}Ba_x)_2CoO_2Cu_2S_2$ at room temperature are shown in Figure 5, obtained from refinements against room-temperature NPD data from POLARIS. Complete substitution of Sr by Ba leads to a 7% increase in *c*, which is more than 3 times greater than the 2% increase in *a*. Expansion of the *a* lattice parameter as Ba^{2+} replaces Sr^{2+} is limited by the maximum Co−O bond length that can be maintained. The *c* parameter, on the other hand, can accommodate much greater expansion. In order to accommodate the larger Ba^{2+} ion between the CoO_2 planes and the puckered Cu_2S_2 layers, the Co−S distance increases by 11%, from its already large value of 3.0327(5) Å in $Sr_2CoO_2Cu_2S_2$ to 3.3721(9) Å in $Ba_2CoO_2Cu_2S_2$. The coordination environment for Co^{2+} thus becomes much more tetragonally elongated, and approaches a CoO_4 square plane, as *x* increases. The Cu−S length remains essentially

dx.doi.org/10.1021/ja109553u |*J. Am. Chem. Soc.* 2011, 133, 2691–2705

Table 2. Results of Structural Refinements for $(Sr_{1-x}Ba_x)_2CoO_2Cu_2S_2$ ($x > 0$) at Room Temperature

radiation			neutron, ToF			Mo Kα, λ = 0.71073 Å
instrument			POLARIS			Nonius FR590 KappaCCD
x in $(Sr_{1-x}Ba_x)_2CoO_2Cu_2S_2$	0.2	0.4	0.6	0.8	1	1
sample	CFS047A	CFS046A	CFS043A	CFS040A	CFS028	CFS037
T/K	298(2)	298(2)	298(2)	298(2)	298(2)	298(2)
space group	*I*4/*mmm*	*I*4/*mmm*	*I*4/*mmm*	*I*4/*mmm*	*I*4/*mmm*	*I*4/*mmm*
a/Å	4.01016(4)	4.02538(4)	4.04013(4)	4.05341(3)	4.06420(3)	4.0711(1)
c/Å	17.9295(2)	18.1680(3)	18.4025(3)	18.6447(2)	18.8870(2)	18.9094(6)
V/Å^3	288.332(8)	294.390(9)	300.378(10)	306.334(4)	311.970(5)	313.40(1)
no. of variables	67	67	67	68	50	16
$R1/R_{wp}$	0.0196	0.0166	0.0133	0.0154	0.0209	0.0178
$wR2/R_{F^2}$	0.0629	0.0680	0.1090	0.0809	0.0417	0.0385
χ^2	1.555	1.086	1.042	0.967	0.843	1.163
Sr/Ba z[a]	0.40735	0.40688	0.40614	0.40514	0.40378(3)	0.40386(1)
S z[a]	0.17272(5)	0.17431(5)	0.17577(5)	0.17705(4)	0.17854(5)	0.17822(5)
F(Cu)[b] refined	1.012(2)	1.017(2)	1.029(3)	0.994(2)	0.975(2)	0.972(4)
F(Cu) from wt fraction	0.989(1)	0.978(1)	0.988(1)	0.978(1)	0.976(1)	–
Sr/Ba $U_{eq} \times 10^2$ (Å^2)	0.65(1)	0.65(1)	0.57(1)	0.65(1)	0.60(1)	0.829(6)
Co $U_{eq} \times 10^2$ (Å^2)	1.07(3)	0.97(4)	1.12(5)	1.07(4)	0.81(2)	0.86(1)
Cu $U_{eq} \times 10^2$ (Å^2)	1.87(2)	1.96(2)	2.06(2)	1.92(2)	1.62(1)	1.81(2)
S $U_{eq} \times 10^2$ (Å^2)	0.86(3)	0.90(4)	0.85(4)	0.91(3)	0.91(2)	1.05(1)
O $U_{eq} \times 10^2$ (Å^2)	0.81(2)	0.88(2)	0.87(2)	0.92(2)	0.89(1)	0.96(3)
Co−O [4][c] (Å)	2.00508(2)	2.01269(2)	2.02006(2)	2.02670(1)	2.03210(2)	2.03560(10)
Co−S [2] (Å)	3.0967(9)	3.1668(9)	3.2348(10)	3.3011(8)	3.3721(9)	3.3700(5)
Sr/Ba−O [4] (Å)	2.6037(3)	2.6293(3)	2.6579(3)	2.6899(3)	2.7261(3)	2.72915(14)
Sr/Ba−S [4] (Å)	3.1783(5)	3.2058(5)	3.2301(5)	3.2501(4)	3.2675(5)	3.2705(4)
Cu−S [4] (Å)	2.4373(5)	2.4376(5)	2.4386(5)	2.4408(4)	2.4395(5)	2.4465(5)
S−Cu−S [2] (°)	110.71(4)	111.31(3)	111.86(4)	112.27(3)	112.82(4)	112.61(4)
S−Cu−S [4] (°)	108.86(2)	108.56(2)	108.29(2)	108.09(2)	107.82(2)	107.924(18)

[a] Co, 2*a*(0,0,0); O, 4*c*(0.5,0,0); Cu, 4d(0.5,0,0.25); Sr/Ba, 4*e*(0,0,*z*); S, 4*e*(0,0,*z*). $Z = 2$. [b] Site occupancy factor of Cu. [c] Numbers in square brackets indicate the multiplicity of each bond or angle.

constant across the series: the Cu_2S_2 layers respond to the expansion in a by a squashing of the CuS_4 tetrahedra in the c direction as the Ba content increases (Figure 5). This flexibility of the Cu_2S_2 layer is presumably important in enabling facile A-site substitution to occur in this structure type. In the similar Fe_2As_2 layers in the iron-based superconductors LnFeAsO, the As−Fe−As angle correlates with the lanthanide radius and seems to be one of the parameters that controls the physical properties.[34] The mean A−O and A−S bond lengths obtained from the refinements do not vary linearly with composition (Figure 5), presumably because we constrained the mixture of Sr and Ba cations to lie on a single site. The refinements are consistent with complete long-range disorder of Sr and Ba on the A cation site, although anisotropic broadening terms in the profile model were required in the refinements, which we assume to be a consequence of short-range ordering of these cations or compositional inhomogeneity (see Supporting Information, Figure S2, for an example). The key structural change is the increasing tetragonal elongation of the Co^{2+} environment, which correlates with the magnetic properties as described below.

Magnetic Properties. *Magnetic Susceptibility Measurements.* Magnetic susceptibility measurements on $Sr_2CoO_2Cu_2S_2$ and $Ba_2CoO_2Cu_2S_2$ (Figure 6) produced results that were consistent with those previously reported.[2,10,11] Prior to air exposure, $Sr_2CoO_2Cu_2S_2$ shows a broad maximum at about 220 K, and $Ba_2CoO_2Cu_2S_2$ shows a similar maximum at 235 K, suggestive of low-dimensional antiferromagnetic ordering of the cobalt sublattice. $Ba_2CoO_2Cu_2S_2$ shows a second maximum at a lower temperature, dependent on the presence of a Curie-like term in the susceptibility at low temperatures, which presumably arises from paramagnetic impurities. The mixed A-site phases $(Sr_{1-x}Ba_x)_2CoO_2Cu_2S_2$ show similar features: broad high-temperature maxima at about 250 K and, for $x \geq 0.6$, secondary maxima between 140 and 170 K (Supporting Information, Figure S6). $Sr_2CoO_2Cu_2S_2$, which has been carefully sequestered from air, also shows divergence of the ZFC and FC susceptibilities below 80 K, consistent with a glassy component to the magnetism. On exposure of $Sr_2CoO_2Cu_2S_2$ to moist air, the behavior of the magnetic susceptibility with temperature changes very significantly, as shown in Figure 6, although the origin of the new features, such as the sharp drop in the susceptibility below 130 K, is not clear. This change, which is reproducible from sample to sample (see Supporting Information, Figure S7), is diagnostic of the degree of degradation. The samples previously reported in the literature have magnetic susceptibilities similar to those of our samples that had not been exposed to air, suggesting that the other reports of the susceptibility were indeed likely measuring material with almost full copper occupancy in the sulfide layer.[2,10] The change in the magnetic susceptibility is at least partially reversible. Annealing of an air-exposed portion of sample CFS126B at 250 °C under vacuum, which was found to increase the cell volume by 0.1% (see above), or treatment under dilute H_2 (5% H_2 in N_2), largely restored the susceptibility of

dx.doi.org/10.1021/ja109553u |*J. Am. Chem. Soc.* 2011, 133, 2691–2705

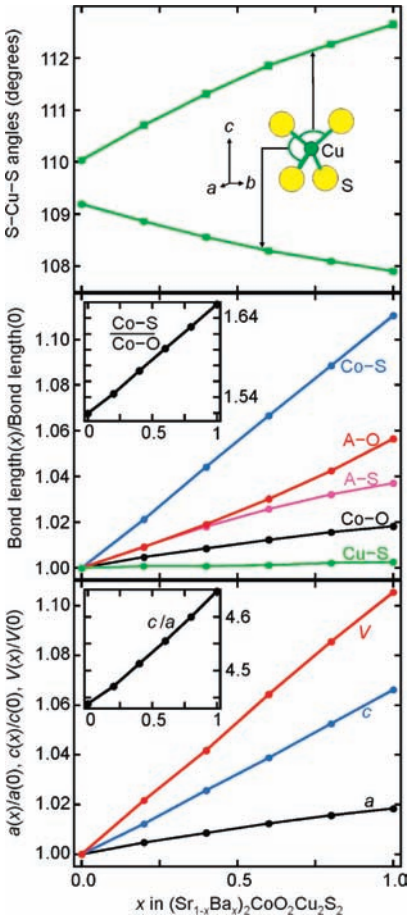

Figure 5. Variation of lattice parameters and selected structural parameters at room temperature with composition in the solid solution $(Sr_{1-x}Ba_x)_2CoO_2Cu_2S_2$. Lines are guides to the eye. Error bars lie within the points.

the pristine material (Figure S7), although these processes also introduced some impurities. This is further evidence that the copper-deficient materials obtained by exposure to moist O_2 are not stable with respect to the stoichiometric material at elevated temperatures. In the reduction experiment using dilute H_2, the CuO that formed on oxidation of the pristine material is presumably reduced and the copper reinserted. This is consistent with the observation that Cu can be reinserted into $CeCu_{1-x}OS$[29] and suggests that the Cu deficiency is diminished on heating the air-exposed and hence copper-deficient material to moderate temperatures. Further measurements will be required to establish the precise origin of the divergence in the unexposed and exposed samples, and there are some reports of unusual behavior in the regime below 80 K.[12,13]

Long-Range Magnetic Ordering. Low-temperature NPD measurements were performed using the constant wavelength diffractometers D1A and D2B at ILL and the ToF diffractometers HRPD, POLARIS, and OSIRIS at the ISIS facility. The magnetic Bragg reflections observed for all samples were indexed, as suggested previously for $Sr_2CoO_2Cu_2S_2$,[2] using a magnetic cell that is a $\sqrt{2}a \times \sqrt{2}a \times c$ expansion of the nuclear cell. The magnetic structure has antiferromagnetic coupling of nearest-neighbor moments within the CoO_2 planes, and the spins in next-nearest-neighbor layers, which are separated by translation by the lattice parameter *c*, are aligned parallel. The

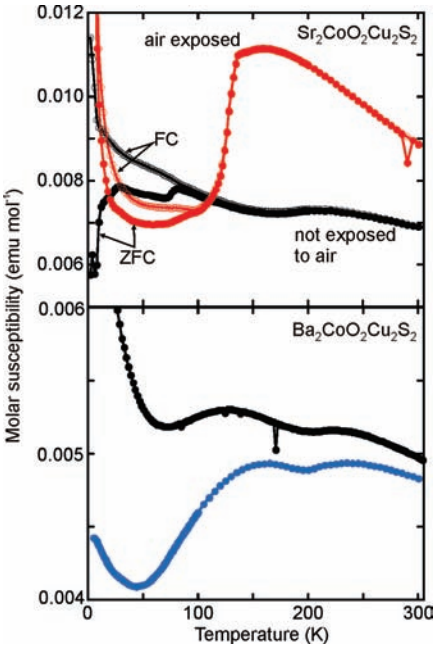

Figure 6. (Top) Magnetic susceptibility of $Sr_2CoO_2Cu_2S_2$ (quenched sample, DRP053) in its pristine form and after exposure to a flow of moist O_2. Zero-field-cooled (ZFC) and field-cooled (FC) measurements made in a measuring field of 100 Oe are shown. (Bottom) Magnetic susceptibilities of two samples of $Ba_2CoO_2Cu_2S_2$ measured in effective applied fields of 1 T.

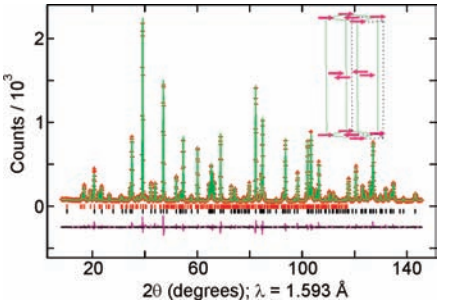

Figure 7. Refinement of the crystal and magnetic structure of $Sr_2CoO_2Cu_2S_2$ (quenched sample DRP053) at 5 K against D2B data. The data (red points), fit (green line), and difference (lower magenta line) are shown together with tic marks indicating nuclear (black) and magnetic (red) reflections. $\chi^2 = 3.96$, $R_{wp} = 0.0629$, and $R(F^2) = 0.0405$. The inset shows the model used for the magnetic structure.

magnetic structural model used for all the compounds described in this paper is shown schematically in Figure 7. We used a magnetic model in *P*1 symmetry with moments arranged collinearly and nearest-neighbor moments antiparallel, but otherwise unconstrained; other models are possible, such as a non-collinear model in which the moments in adjacent antiferromagnetic planes are rotated by 90° with respect to one another in the basal plane,[35] but these models are indistinguishable using a powder diffraction measurement. The moments lie mainly in the basal plane, with a small component directed along the *z* axis.

$Sr_2CoO_2Cu_2S_2$. The samples DRP051 (slow-cooled) and DRP053 (quenched) described above were both measured on the D2B diffractometer. Refinement of the ordered moment on the cobalt ions (Figure 7) revealed that, in the portions of each

Table 3. Refined Co^{2+} Magnetic Moment Components from NPD Data at 5 K

compound	sample	instrument	M_x (μ_B)	M_y (μ_B)	M_z (μ_B)	$\|M\|$ (μ_B)
$Sr_2CoO_2Cu_2S_2$	DRP051 (slow-cooled, unexposed)	D2B	2.94(7)	2.39(8)	0.4(5)	3.81(6)
$Sr_2CoO_2Cu_2S_2$	DRP051 (slow-cooled, exposed to moist O_2)	D2B	2.0(1)	2.0(1)	1.0(3)	3.0(1)
$Sr_2CoO_2Cu_2S_2$	DRP053 (quenched, unexposed)	D2B	2.85(7)	2.42(7)	0.9(2)	3.85(6)
$Sr_2CoO_2Cu_2S_2$	DRP053 (quenched, exposed to moist O_2)	D2B	1.6(1)	1.6(1)	0.9(2)	2.44(6)
$Ba_2CoO_2Cu_2S_2$	CFS071B	D2B	3.05(9)	3.01(9)	1.2(2)	4.45(9)
$Ba_2CoO_2Cu_2S_2$	CFS044A	HRPD	2.92(2)	3.21(2)	1.32(4)	4.53(1)

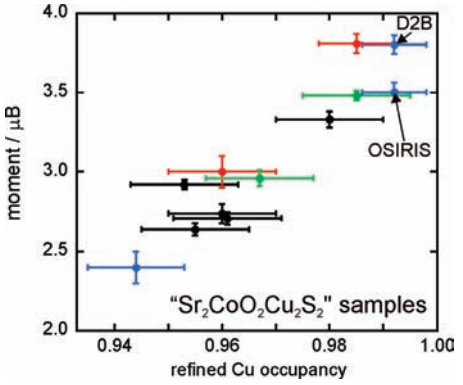

Figure 8. Plot of refined Cu site occupancy against ordered magnetic moment from neutron diffraction measurements on several "$Sr_2CoO_2Cu_2S_2$" samples. Samples DRP051 (red) and DRP053 (blue) were synthesized stoichiometrically. Sample CFS127C (green) was synthesized as "$Sr_2CoO_2Cu_{1.85}S_2$". For these three samples, measurements were made both with no air exposure and after controlled exposure to a flow of moist O_2.

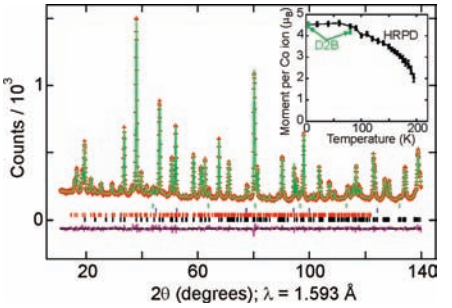

Figure 9. Refinement of the crystal and magnetic structure of $Ba_2CoO_2Cu_2S_2$ (*Immm*) against D2B NPD data collected at 5 K. Positions of nuclear and magnetic reflections are given by black and red tic marks, respectively; blue and green correspond to scattering from elemental Cu and the vanadium sample holder. $\chi^2 = 1.947$, $R_{wp} = 0.0326$, and $R(F^2) = 0.0477$. The inset shows the temperature dependence of the moment obtained from refinements against D2B and HRPD data. The poor fit to the low-temperature D2B data in *I*4/*mmm* is shown in the Supporting Information, Figure S4.

sample that had received no air exposure, the ordered moments were both 3.8(1) μ_B. The refined components of the moments are listed in Table 3. The unexposed portion of sample DRP053 was also measured using the OSIRIS diffractometer, and the refined moment from this data set was 3.5(1) μ_B, 8(5)% smaller than the value from D2B. We presume that this discrepancy arises from the correlation of the refined ordered moment with sample absorption. On exposure to moist oxygen, simulating moist air, which we have shown above results in a Cu deficiency and significant changes in the magnetic susceptibility, the ordered moments of the two samples DRP051 and DRP053 measured on D2B decreased significantly to 3.0(1) and 2.4(1) μ_B, respectively. The magnetic model used remained unchanged, and there is little effect on the orientation of the moment. In the course of our investigations of the possibility of synthesizing copper-deficient samples $Sr_2CoO_2Cu_{2-\delta}S_2$, and in investigating the sensitivity of $Sr_2CoO_2Cu_2S_2$ to ambient air and to a moisture-laden O_2 flow, we gathered several neutron diffractograms from which we can refine both the ordered moment and the copper site occupancy (see Table S1 in the Supporting Information for further details of these samples). These results reveal an approximately linear dependence of the ordered moment against refined copper site occupancy, as shown in Figure 8.

The long-range ordered moment of about 3.8(1) μ_B in $Sr_2CoO_2Cu_2S_2$ phases that are no more than 1% deficient in Cu shows that there is a very significant orbital contribution to the magnetic moment of Co^{2+} ($S = 3/2$) in a highly tetragonally distorted CoO_4S_2 coordination environment, and we return to this point below. A decrease in the ordered moment on oxidation by moist O_2 is expected: oxidation of up to 10% of the Co^{2+} ions to Co^{3+} should lead to a reduced moment per Co ion, even if the ion remains high spin, and disorder between Co^{2+} and Co^{3+} species would also reduce the long-range ordered moment that is measured in a diffraction experiment. It is also plausible that some of the Co 3d electrons become itinerant on oxidation, reducing the local moment, but our current measurements do not allow us to disentangle these possible contributions.

$Ba_2CoO_2Cu_2S_2$. PND measurements on $Ba_2CoO_2Cu_2S_2$ carried out on D2B (Figure 9) and HRPD revealed magnetic reflections visible below 210 K, which reached saturation below about 80 K. In this case, the refined magnetic moment at 5 K was 4.5 μ_B for both sample CFS071B measured on D2B and sample CFS044A measured on HRPD (Table 3). The moment obtained for $Ba_2CoO_2Cu_2S_2$ is at least 0.7 μ_B larger than that obtained for unexposed samples of $Sr_2CoO_2Cu_2S_2$ and, therefore, very much larger than the spin-only moment, indicating that there is an even larger orbital contribution to the moment in $Ba_2CoO_2Cu_2S_2$, with a more tetragonally elongated Co^{2+} environment. We note here that the room-temperature *I*4/*mmm* structural model for $Ba_2CoO_2Cu_2S_2$ was found to fit the D2B data poorly at low temperatures (Supporting Information, Figure S4), and a reduction in symmetry to *Immm*, but retaining the unit cell volume, was required to model the data ($a = 4.0466(3)$, $b = 4.0602(3)$, and $c = 18.755(2)$ Å at 5 K; Supporting Information, Table S2). We consider this structural distortion in more detail below.

$(Sr_{1-x}Ba_x)_2CoO_2Cu_2S_2$. Several samples were measured on the ToF diffractometers OSIRIS and HRPD at ISIS. Low-temperature HRPD data, from which we obtained structural information (see below), have a poor signal-to-noise ratio at low Q but were used to define the nuclear structural model in the

dx.doi.org/10.1021/ja109553u |*J. Am. Chem. Soc.* 2011, 133, 2691–2705

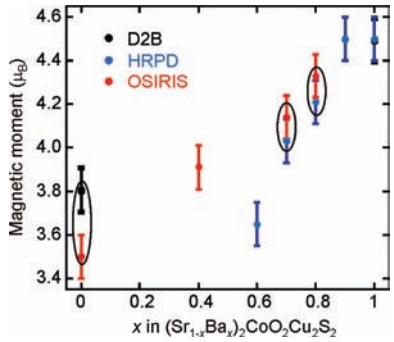

Figure 10. Variation of refined long-range ordered moment on Co as a function of composition for the series $(Sr_{1-x}Ba_x)_2CoO_2Cu_2S_2$. Three samples were measured on two diffractometers, as indicated by the ovals linking the points.

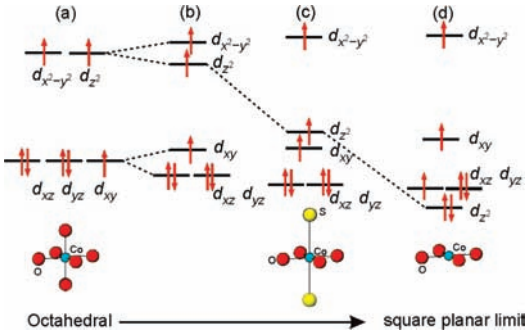

Figure 11. Cartoon showing the d orbital splitting for molecular high-spin Co^{2+} systems ranging from purely octahedral (a) to purely square planar (d) via a slightly tetragonally elongated octahedron (b) and the highly tetragonally elongated arrangement appropriate to $Sr_2CoO_2Cu_2S_2$ (c). (Note that, as far as we are able to ascertain, the purely square planar *high-spin* Co^{2+} system has not been realized experimentally in a molecular system.) The $d_{x^2-y^2}$ and d_{z^2} orbitals are σ-antibonding, and the d_{xy}, d_{xz}, and d_{yz} orbitals are π-antibonding.

refinements against OSIRIS data on some of the same samples (Supporting Information, Figure S3). Data from OSIRIS offer extremely high signal-to-noise ratios and resolution at low Q and enable small CoO impurities that were not evident in the nuclear refinements to be observed (Figure S3), but the high Q data are not optimal for defining the structural model for these compounds with small unit cells. The values of the refined magnetic moments are somewhat correlated with the diffractometer used for the refinement, as discussed for $Sr_2CoO_2Cu_2S_2$ above, but using realistic uncertainties in the values of the ordered moments, analysis of several samples of $(Sr_{1-x}Ba_x)_2CoO_2Cu_2S_2$ revealed that there was an approximately linear increase in the size of the ordered moment with increasing Ba content, as shown in Figure 10.

Orbital Enhancements of the Moment in Co^{2+} Compounds. It is well-known that high-spin d^7 Co^{2+} ions in octahedral coordination carry an unquenched orbital contribution to the magnetic moment arising from the $^4T_{1g}$ ground term.[36] In the case of a small distortion of a CoO_6 octahedron from O_h symmetry by axial elongation, the octahedral $^4T_{1g}$ ground term splits into a lower-lying $^4A_{2g}$ ground term and a higher-lying ^4E_g term in D_{4h} symmetry. The $^4A_{2g}$ ground term cannot carry a first-order orbital moment, but there will remain an orbital contribution to the moment through the mixing-in of higher lying ^4E_g terms via spin−orbit coupling. The size of the orbital contribution to the moment will diminish as the size of the term splitting increases relative to the spin−orbit coupling parameter. It is perhaps convenient to consider the situation in terms of the familiar 3d orbitals: axial elongation lifts the degeneracy of the octahedral e_g and t_{2g} sets of orbitals. Of the σ-antibonding (e_g in octahedral symmetry) orbitals, $d_{x^2-y^2}$, which is σ-antibonding with respect to the equatorial ligands, will be destabilized, while d_{z^2} will be stabilized. Of the π-antibonding (t_{2g} in octahedral symmetry) orbitals, d_{xy} will be destabilized because it is π-antibonding with respect to all four equatorial ligands, while d_{xz} and d_{yz}, which are each antibonding with respect to only two of the equatorial ligands and to the two axial ligands, will be stabilized. For a slightly axially elongated high-spin Co^{2+} d^7 ion, the configuration is therefore expected to be $(d_{xz},d_{yz})^4(d_{xy})^1(d_{z^2})^1(d_{x^2-y^2})^1$, as shown schematically in Figure 11b. In the $(Sr_{1-x}Ba_x)_2CoO_2Cu_2S_2$ series, there are clearly large orbital enhancements to the magnetic moments, and the size of the magnetic moment increases as the degree of tetragonal elongation of the Co^{2+} environment increases: both the ordered moment and the (Co−S)/(Co−O) ratio vary approximately linearly with x in $(Sr_{1-x}Ba_x)_2CoO_2Cu_2S_2$, as shown in Figures 10 and 5, respectively.

Computation. We have carried out first-principles electronic structure calculations of the stoichiometric $Sr_2CoO_2Cu_2S_2$ and $Ba_2CoO_2Cu_2S_2$ to gain insight into the magnetic behavior of these nonmolecular compounds using an on-site Coulombic correction in terms of the Hubbard term U to describe the 3d electron−electron repulsion of the cobalt cation. Different values of U were tested. Results for the case U = 3 eV are shown. The inclusion of the U parameter was found to stabilize strongly the observed antiferromagnetic ground state over an alternative ferromagnetic ground state for both compounds, by 0.42 eV in $Sr_2CoO_2Cu_2S_2$ and 1.73 eV in $Ba_2CoO_2Cu_2S_2$. If this parameter was not included in the calculations (i.e., U = 0), the ferromagnetic state was favored by 0.53 eV for $Sr_2CoO_2Cu_2S_2$ and 0.74 eV for $Ba_2CoO_2Cu_2S_2$.

The total electronic densities of states (EDOS) for the two compounds with U = 3 eV are compared in Figure 12 (results for $Sr_2CoO_2Cu_2S_2$ showing the opening of the gap at E_F as U is increased are included in the Supporting Information, Figure S8). The site-projected EDOS for $Sr_2CoO_2Cu_2S_2$ is also shown in Figure 12. Clearly, the top of the valence band is composed of well-mixed Co 3d/O 2p states and Cu 3d/S 3p states, so our conjecture above—that the changes in Cu−S, Co−O, and Co−S bond lengths when $Sr_2CoO_2Cu_2S_2$ is subjected to mild oxidation result from oxidation of the Cu 3d/S 3p states and the mainly Co 3d states—is supported by the calculations. The suggestion in ref 12 that there is a temperature-dependent electron transfer between the CoO_2 and Cu_2S_2 layers is also certainly not implausible from our calculations, although it is not clear whether the sample in ref 12 is stoichiometric or slightly copper-deficient as a result of air exposure.

Consider in more detail the projection of the Co 3d EDOS. Figure 13 compares the results for $Sr_2CoO_2Cu_2S_2$ and $Ba_2CoO_2Cu_2S$, which show that the effect of increasing the tetragonal elongation of the CoO_4S_2 octahedron is profound. In $Sr_2CoO_2Cu_2S_2$, the result is that the α spin EDOS lies below E_F, while the β components of d_{z^2}, d_{xy}, and $d_{x^2-y^2}$ are unoccupied (above E_F). This situation corresponds to the configuration derived above and shown in Figure 11b,c. In the case of $Ba_2CoO_2Cu_2S_2$, the calculations show a slightly different picture (Figure 13). With

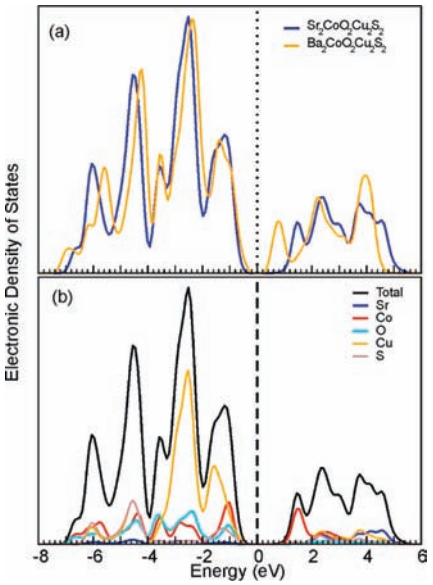

Figure 12. (a) Total electronic density of states for $Sr_2CoO_2Cu_2S_2$ and $Ba_2CoO_2Cu_2S_2$ for U = 3 eV. (b) Total and site-projected EDOS for $Sr_2CoO_2Cu_2S_2$ obtained for the antiferromagnetic magnetic spin configuration with U = 3 eV.

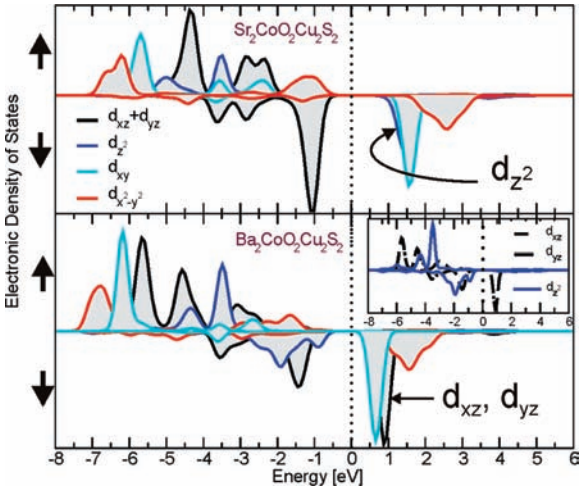

Figure 13. Angular-momentum-resolved EDOS for the Co 3d levels (l = 2) for $Sr_2CoO_2Cu_2S_2$ (top) and $Ba_2CoO_2Cu_2S_2$ (bottom).

the increased tetragonal elongation of the CoO_4S_2 octahedron, the picture that emerges from the calculations is that now the d_{z^2} β spin component is occupied, while the d_{xz} and d_{yz} β components are only half occupied. There is also greatly increased mixing of the d_{z^2} and d_{xz},d_{yz} spin orbitals compared with the $Sr_2CoO_2Cu_2S_2$ case. The calculations suggest that, in our simple ligand field picture, the $Ba_2CoO_2Cu_2S_2$ system is very close to the crossover from the $^4A_{2g}$ (Figure 11c) to the ^4E_g (Figure 11d), and the d_{z^2} is very close to degenerate with d_{xy} and d_{xz}.

The environment for high-spin Co^{2+} in oxide systems ranges from almost purely octahedral in CoO to approximately square planar (i.e., highly tetragonally elongated octahedral) in the layered oxysulfides described here and in related oxyhalides such as $Sr_2CoO_2X_2$ (X = Cl, Br).[37] In CoO, which has the rock salt structure, the magnitude of the ordered magnetic moment is about 4 μ_B.[38,39] The spin-only moment expected for high-spin Co^{2+} is 3 μ_B, but in a collective magnetic system, the value of the ordered moment measured by neutron diffraction tends to be reduced by covalency,[40] so CoO has a very large orbital moment in excess of 1 μ_B. A small axial compression of the octahedron in CoO accompanying the cubic-to-monoclinic distortion below 290 K[38] results in $r(Co-O)_{ax}/r(Co-O)_{eq}$ = 0.99, and the ground term should retain the orbital contribution to the moment.

In La_2CoO_4, which has tetragonal symmetry at low temperatures,[35] there is distortion from octahedral symmetry about Co^{2+} via axial elongation ($^4A_{2g}$ ground term) such that $r(Co-O)_{ax}/r(Co-O)_{eq}$ = 1.05 (i.e., similar to Figure 11b). The low-temperature ordered moment is 2.9 ± 0.1 μ_B,[35] which suggests that only a small orbital contribution is retained by mixing-in of excited ^4E_g terms. Similar ordered moments for distorted octahedral Co^{2+} ions are 3.0 ± 0.1 μ_B in both $La_2Co_2O_5$[41] and $La_4Co_3O_9$[42] (both orthorhombic), in which the CoO_6 polyhedra are distorted to a slightly larger extent than in La_2CoO_4, with four short distances of 1.93−2.03 Å and two longer distances of about 2.25 Å. In the current oxysulfide systems, there is a much larger axial anisotropy than in these oxide systems (Figure 11c), and the coordination environment for Co^{2+} approaches square planar, as noted in the title of the original communication.[2] The data presented here show that, far from the orbital moment being quenched completely by this extreme distortion from octahedral symmetry, the orbital contribution in $Ba_2CoO_2Cu_2S_2$, which has the most tetragonally elongated (i.e., closest to square planar) coordination environment we are aware of for a high-spin Co^{2+} ion, is even larger than that in CoO. The significant unquenched orbital moment in similar systems is also noted by Knee et al. in the compounds $Sr_2CoO_2X_2$ (X = Cl, Br),[37] which are formally related to the oxysulfides by replacement of the chalcogenide ion by a halide and removal of the Cu^+ ions from the nonoxide layer. These compounds are reported to exhibit magnetic structures similar to those of the oxysulfides described here. Our calculations (see Figure 13) suggest that, in $Ba_2CoO_2Cu_2S_2$, we may have approached the point indicated by Figure 11d, where the d_{z^2} is the least antibonding orbital. Square planar systems are known for Co^{2+}, and Ceulemans et al.[43] considered Co^{2+}−Schiff base compounds, which are low-spin because of the higher ligand field from N ligands. In those systems, spectroscopic data and reasonable values for the Racah parameters B and C were used to estimate the relative energies of the d orbitals. The analysis of this molecular system showed that the $3d_{z^2}$ orbital was of lowest energy and was estimated to be approximately nonbonding as a result of mixing with the Co 4s orbital; the π-type antibonding orbitals were located approximately 2000 cm^{-1} (0.25 eV) (d_{xz},d_{yz}) and 4000 cm^{-1} (0.5 eV) (d_{xy}) higher, with the $d_{x^2-y^2}$ σ-antibonding orbital approximately 20 000 cm^{-1} (2.5 eV) higher. In the oxysulfide and oxyhalide cases, the axial ligands are not completely removed. Demazeau et al.,[44] in considering octahedral distortions in K_2NiF_4-type compounds, estimated that the ligand field strength falls off roughly as r^{-5}, where r is the internuclear distance. In $Ba_2CoO_2Cu_2S_2$, the interatomic distances are $r_{Ba}(Co-S)$ = 3.37 Å and $r_{Ba}(Co-O)$ = 2.03 Å. The radius of S^{2-} exceeds that of O^{2-} by about $r_{S-O} \approx$ 0.4 Å according to standard tables,[45] so the ratio of the axial and equatorial ligand field strengths will be roughly $\sigma_{ax}/\sigma_{eq} = [(r_{Ba}(Co-S) - r_{S-O})/r_{Ba}(Co-O)]^{-5} = [(3.37-0.4)/2.03]^{-5} \approx 0.15$. Bearing in mind that sulfide is a weaker field ligand than

oxide and that we are making several assumptions, we estimate that, as a result of the weak σ-type axial ligand field of the sulfide, the d_{z^2} orbital will be raised relative to its energy in the purely square planar case by about 10% compared with the $d_{x^2-y^2}$ orbital. The net result, following the result of Ceulemans et al.,[43] is that d_{z^2} is expected to be close to degenerate with $d_{xz,yz}$, and these three orbitals will have one hole between them in a high-spin d^7 system. This is consistent with the picture that emerges from our calculations. Spin−orbit coupling mixes d_{z^2} with $d_{xz,yz}$ to an extent that depends on the energy separation of the levels, and since the orbitals are close to degenerate in energy, we propose that this is the origin of the very large orbital contribution to the moment in $Ba_2CoO_2Cu_2S_2$. It is unclear whether the ground term in this case is ^4E_g [corresponding to the configuration $(d_{z^2})^2(d_{xz},d_{yz})^3(d_{xy})^1(d_{x^2-y^2})^1$] with a first-order orbital moment or $^4A_{2g}$ [corresponding to the configuration $(d_{xz},d_{yz})^4(d_{z^2})^1(d_{xy})^1(d_{x^2-y^2})^1$] with the ^4E_g close in energy. In $Sr_2CoO_2Cu_2S_2$ and the oxyhalides $Sr_2CoO_2Cl_2$ and $Sr_2CoO_2Br_2$,[37] the anisotropy is smaller, and we estimate that $\sigma_{ax}/\sigma_{eq} = [(r_{Sr}(Co-S) - r_{S-O})/r_{Sr}(Co-O)]^{-5} = [(3.01-0.4)/1.99]^{-5} \approx 0.25$, which, following Ceulemans et al.,[43] would place d_{z^2} above $d_{xz,yz}$ by about 2000 cm^{-1} (0.25 eV) and roughly degenerate with d_{xy} (i.e., Figure 11c), which seems to be borne out by our calculations (Figure 13). The many-electron spin−orbit coupling parameter, λ, for Co^{2+} is around −200 cm^{-1} (−25 meV), so the mixing of the orbitals in $Sr_2CoO_2Cu_2S_2$ will be significantly less than in the case of $Ba_2CoO_2Cu_2S_2$, and the orbital moment will be correspondingly reduced. Finally, delocalization onto the ligands tends to reduce the spin and orbital moments.[40] As the Co−O distance increases, this reduction is expected to decrease further, enhancing the ordered moment, and this may partially account for the larger ordered moment in $Ba_2CoO_2Cu_2S_2$.

Calculations were also performed in which spin−orbit coupling was included (Supporting Information, Table S3). These showed two things: First, there is a strong in-plane magnetic anisotropy in these systems, consistent with the experimental observation that the magnetic moments have their major component oriented in the CoO_2 planes. Second, the calculations showed qualitatively that the orbital component of the magnetic moment should be larger in the case of $Ba_2CoO_2Cu_2S_2$ than $Sr_2CoO_2Cu_2S_2$, although the difference in the size of the experimental moments of about 0.7 μ_B is about a factor of 5 larger than that suggested by the calculations, as is commonly found in comparable computations due to the nature of the numerical integration in these calculations.[46] The calculations predict a larger z component of the magnetic moment in $Ba_2CoO_2Cu_2S_2$ than in $Sr_2CoO_2Cu_2S_2$, and the data in Table 3 support this, although the uncertainties are large in the M_z values.

A survey of all the literature examples we can find with Co^{2+} in octahedral or axially distended environments reveals a sharp decrease in the size of the long-range ordered magnetic moment on distortion from octahedral symmetry, followed by a smooth increase with the ratio of the axial Co−X (X = oxide, halide, chalcogenide) distance and the equatorial Co−O distance. This is shown in Figure 14.

Low-Temperature Structural Distortions. As indicated above, the measurements of $Ba_2CoO_2Cu_2S_2$ on D2B at 5 and 80 K revealed poorly resolved peak splittings in the high-angle (~120° 2θ) region of the diffractogram (Supporting Information, Figure S4), suggesting a structural distortion of the room-temperature tetragonal cell. The D2B data were modeled adequately using an orthorhombic cell in *Immm* with a volume similar to that of the room-temperature tetragonal cell in *I*4/*mmm*. We subsequently

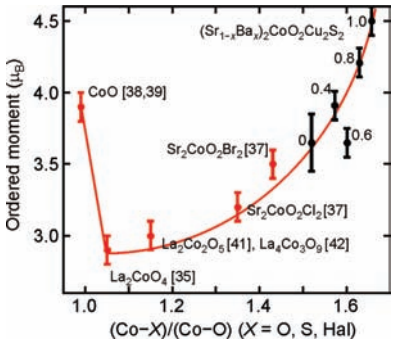

Figure 14. Changing magnetic moment of Co^{2+} as a function of the Co coordination geometry in various solid-state compounds from the literature (red) and from this work (black). Literature values are used for the bond lengths in the oxides[35,38,39,41,42] and oxyhalides,[37] with average values for the axial (×2) and equatorial (×4) Co−O bond lengths for systems with lower than D_{4h} symmetry at Co^{2+}.[41,42] The line is a guide to the eye.

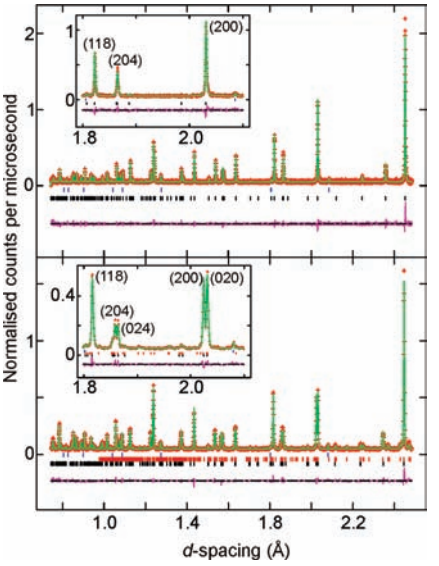

Figure 15. Refinements of $Ba_2CoO_2Cu_2S_2$ against HRPD NPD data collected at 250 and 4 K (165° detector bank). Positions of nuclear and magnetic reflections are given by black and red tic marks, respectively; blue tic marks correspond to scattering from the small amount of elemental Cu in the sample.

measured the diffraction pattern of a second sample of $Ba_2CoO_2Cu_2S_2$ (CFS044A) between 4 and 250 K using the higher resolution diffractometer HRPD at the ISIS facility, which revealed that the distortion is evident only below about 155 K, somewhat below the temperature of 210 K at which long-range 3D magnetic ordering is apparent from the appearance of magnetic Bragg reflections. The refinements were consistent with an orthorhombic distortion of the crystal structure, and the splitting of, for example, the 200/020 reflections was well-resolved using the highest resolution backscattering detector bank on HRPD. The results of Rietveld refinement against the HRPD data are shown in Figure 15 and in the Supporting Information, Table S2. Attempts to establish whether the symmetry was further reduced from *Immm* at low temperatures were hampered by beam heating of the sample on ID31.

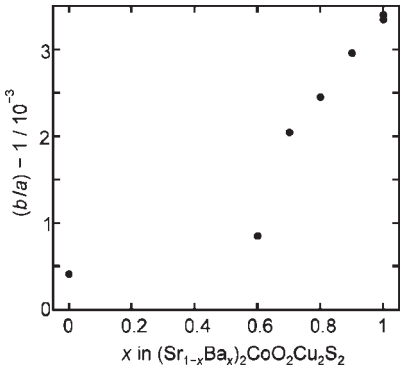

Figure 16. Size of the orthorhombic distortion in $(Sr_{1-x}Ba_x)_2CoO_2Cu_2S_2$ samples measured on ID31 (x = 0), D2B (one sample with x = 1), or HRPD.

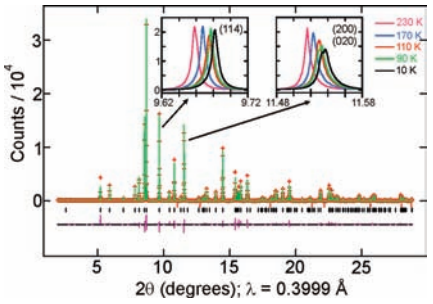

Figure 17. Rietveld refinement against ID31 data at 10 K of a sample of $Sr_2CoO_2Cu_2S_2$ (DRP051) that had not been exposed to air. The insets show the evolution of the orthorhombic distortion: the tetragonal (200) splits at low temperatures, while the width of the (114) reflection is temperature-independent.

We used HRPD to probe the presence of the low-temperature structural distortion in the members of the $(Sr_{1-x}Ba_x)_2CoO_2Cu_2S_2$ series. For x = 0.9, the 200 and 020 reflections of the orthorhombic *Immm* low-temperature cell are clearly resolved. For smaller values of x, these reflections are not completely resolved, even in backscattering, although the peaks are broader than at ambient temperature, and stable refinements were achieved using the orthorhombic model, showing a linear decrease in the size of the distortion with decreasing Ba content (Figure 16), with an unusually low value of the distortion in the sample with x = 0.6.

Subsequently we analyzed samples of $Sr_2CoO_2Cu_2S_2$ using high-resolution diffraction data. The two portions of sample DRP051 (slow-cooled sample, one portion unexposed to air, and the other exposed to a flow of moist oxygen) were measured on ID31 between 10 and 290 K. The high-resolution data showed a clear orthorhombic distortion at 130 K and below in the unexposed portion of the sample (Figure 17). At 150 K, the *Immm* model and the alternative *I*4/*mmm* model gave fits that were of similar statistical quality, although the orthorhombic model failed to converge, so we conclude that the tetragonal model is appropriate at 150 K. The variation of the basal lattice parameters with temperature for $Sr_2CoO_2Cu_2S_2$ is compared with that of $Ba_2CoO_2Cu_2S_2$ in Figure 18, where the lattice parameters have been normalized to their values at 210 K for each compound. As described above (Figure 2), the exposure of $Sr_2CoO_2Cu_2S_2$ to moist O_2 results in a broadening of all the reflections that is somewhat asymmetric. This hampered the

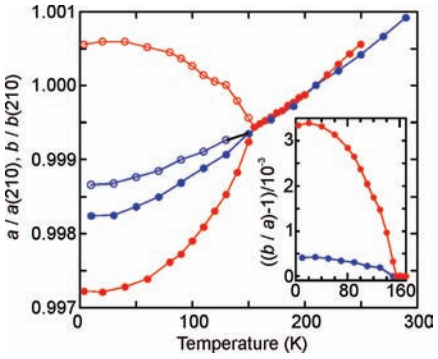

Figure 18. Temperature dependence of the lattice parameters of $Sr_2CoO_2Cu_2S_2$ (DRP051 not air-exposed) (blue) and $Ba_2CoO_2Cu_2S_2$ (CFS044) (red). The values of the lattice parameters (a, filled symbols; b, open symbols) have been normalized to their values at 210 K (3.98789(2) Å for $Sr_2CoO_2Cu_2S_2$ and 4.05860(1) Å for $Ba_2CoO_2Cu_2S_2$). The inset shows that the distortion (expressed as $(b/a) - 1$) is almost an order of magnitude larger in $Ba_2CoO_2Cu_2S_2$ than in $Sr_2CoO_2Cu_2S_2$.

analysis of the low-temperature structure of the exposed material, although the orthorhombic model remains marginally superior to the tetragonal model at low temperatures, so it seems that the air exposure does not quench the structural distortion in this sample. (Figure S5 in the Supporting Information shows that the low-temperature broadening of the 114 and 200 reflections is qualitatively similar to that shown in Figure 17.)

Gathering together our results on samples of $(Sr_{1-x}Ba_x)_2CoO_2Cu_2S_2$ across the entire solid solution, we see a fairly smooth and approximately linear variation in the size of the low-temperature distortion with x for samples that have received no air exposure (Figure 16). Following our observation of a similarly smooth variation of the size of the ordered moment with composition for unexposed samples (Figure 10), we can plot the size of the distortion, $(b/a) - 1$, determined from high-resolution diffraction measurements against the size of the ordered moment determined from low-temperature neutron diffraction measurements (Figure 19). Included in this plot are the results for all the samples of "$Sr_2CoO_2Cu_2S_2$" for which we have measurements of the ordered moment and diffraction data at high enough resolution (ID31 or HRPD) to enable the distortion to be discerned. Some of these had received some air exposure, and others had been synthesized at the composition $Sr_2CoO_2Cu_{1.85}S_2$ and contain impurities. For $Ba_2CoO_2Cu_2S_2$, we have measured the sizes of the distortion (Figure 18) and the ordered moment (Figure 9) in our HRPD experiment, and these data are also plotted in Figure 19. The onset of the distortion does not coincide with the first appearance of magnetic Bragg peaks but is evident once the long-range ordered moment has grown larger than about 3.3 μ_B.

When there is collinear ordering of magnetic moments that have an orbital component, the effect of the spin−orbit coupling is to induce a small cooperative crystallographic distortion at or below the temperature at which long-range magnetic ordering occurs.[47] We propose that such a magnetostrictive distortion occurs in $(Sr_{1-x}Ba_x)_2CoO_2Cu_2S_2$. The distortion we observe is evident at temperatures somewhat below T_N. The moments in $(Sr_{1-x}Ba_x)_2CoO_2Cu_2S_2$ are oriented mainly in the basal plane, so an in-plane magnetostrictive distortion is expected. If we assume that the spin contribution to the magnetic moment of Co^{2+} in these systems remains constant, then the fact that the

dx.doi.org/10.1021/ja109553u |*J. Am. Chem. Soc.* 2011, 133, 2691–2705

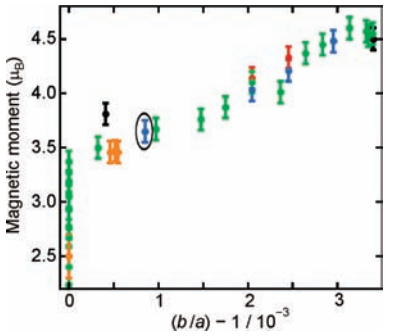

Figure 19. Dependence of the long-range ordered magnetic moment on the size of the orthorhombic distortion for samples $(Sr_{1-x}Ba_x)_2CoO_2Cu_2S_2$. The color coding indicates the diffractometer used for the determination of the magnetic moment (black, D2B; blue, HRPD; red, OSIRIS) as in Figure 10. Green symbols denote the variable-temperature data on $Ba_2CoO_2Cu_2S_2$ (HRPD), and orange symbols indicate samples of nominal composition $Sr_2CoO_2Cu_{1.85}S_2$, some of which had received exposure to moist air. The sample of $(Sr_{1-x}Ba_x)_2CoO_2Cu_2S_2$ with $x = 0.6$, which is an apparent outlier in Figures 10 and 16, is ringed.

orbital contribution to the long-range ordered moment increases with increasing Ba content is consistent with the observation that the size of the magnetostrictive distortion also increases with increasing Ba content. Further evidence that the distortion is driven by the magnetic ordering lies in the sample with $x = 0.6$. This is an outlier in the plots of moment versus composition (Figure 10) and distortion versus composition (Figure 16). However, this point (ringed in Figure 19) lies on the trend of ordered moment against distortion exhibited by the other samples. A distortion of magnitude similar to that in $Ba_2CoO_2Cu_2S_2$ occurs below the charge-ordering Verwey transition in Fe_3O_4, in which the localized Fe^{2+} ions carry an orbital magnetic moment.[48] In CoO there is a distortion below T_N that has as its main component a tetragonal compression of the octahedron by about 1.2%. A further smaller component of the distortion renders the symmetry monoclinic.[38] The largest orthorhombic distortion that we observe below T_N in the $(Sr_{1-x}Ba_x)_2CoO_2Cu_2S_2$ series is similar in size to the smaller (trigonal) component of the distortion in CoO.

CONCLUSIONS

The series of compounds $(Sr_{1-x}Ba_x)_2CoO_2Cu_2S_2$ are rare examples of systems with high-spin Co^{2+} ions in a coordination environment that is a highly distorted CoO_4S_2 octahedron, so the environment for Co^{2+} is close to being purely square planar. The systems order antiferromagnetically with the moments mainly oriented in the basal plane, as predicted by computational studies. The size of the long-range ordered magnetic moment carried by the Co^{2+} ion increases as the CoO_4S_2 polyhedron becomes increasingly tetragonally elongated with increasing x (increasing Ba content). Computational analysis of the end member compounds ($x = 0$ and 1) and consideration of the calculated 3d manifold in molecular Co^{2+} systems show that this behavior is consistent with the decreasing separation with increasing x of unequally occupied 3d levels that are coupled by the spin−orbit interaction. Thus, the orbital component of the moment carried by the Co^{2+} ion increases as the Ba content increases, and the Co^{2+} environment becomes more tetragonally elongated. The size of the low-temperature long-range ordered magnetic moment in a range of Co^{2+} solid-state compounds correlates strongly with the coordination environment, ranging from a slightly tetragonally elongated octahedron in La_2CoO_4 to highly elongated, and almost purely square planar, in $Ba_2CoO_2Cu_2S_2$ (Figure 14). Furthermore, the fact that the ordered magnetic moments in $(Sr_{1-x}Ba_x)_2CoO_2Cu_2S_2$ have their major component oriented in the CoO_2 plane results in a magnetostrictive distortion of the CoO_2 planes that is evident at temperatures below the long-range ordering transition temperature. The size of this distortion correlates well with the size of the ordered moment, and in $Sr_2CoO_2Cu_2S_2$ the distortion is close to the resolution limit of even the highest resolution powder diffractometers (Figure 19). A final important observation is that $Sr_2CoO_2Cu_2S_2$ is rather unobtrusively air-sensitive. We have shown that this compound is subject to oxidative de-intercalation of copper through aerial oxidation, with the formation of a 5% copper deficiency and poorly crystalline CuO coexisting with the oxidized oxysulfide phase. This oxidation has a significant effect on the size of the ordered magnetic moment, which may be ascribed, at least in part, to the formation of Co^{3+} ions that carry a lower moment than Co^{2+} ions. Whether partial frustration of long-range magnetic order by Co^{2+}/Co^{3+} disorder or itinerant behavior of some of the Co 3d electrons accompanies oxidation remains to be investigated. In the absence of statements to the contrary, we assume that the physical measurements that noted unusual behavior of $Sr_2CoO_2Cu_2S_2$[12,13] were made on samples exposed to air, which may be closer to $Sr_2CoO_2Cu_{1.9}S_2$ or may have changed their composition during their examination; we anticipate that some re-evaluation of the previously reported physical properties of this compound may be required, not least because the partial oxidative de-intercalation of copper evidently has a significant effect on the magnetic susceptibility and on the size of the long-range ordered moment, as we describe. The changes in other physical properties, such as conductivity and thermopower, with composition may also be very significant.

ASSOCIATED CONTENT

Supporting Information. Further tables of refinement parameters, diffractograms showing Rietveld refinements, crystallographic information files, magnetic susceptibility data, and computational output. This material is available free of charge via the Internet at http://pubs.acs.org.

AUTHOR INFORMATION

Corresponding Author
simon.clarke@chem.ox.ac.uk

ACKNOWLEDGMENT

We thank the UK Engineering and Physical Sciences Research Council for funding under grant EP/E025447 and for the award of a studentship to C.F.S. We are grateful to Dr. R. I. Smith, Dr. K. Knight, Dr. R. M. Ibberson, Dr. M. Telling (ISIS facility), Dr. A. Hewat, and Dr. E. Suard (ILL, Grenoble) for assistance with the PND measurements, and Dr. A. N. Fitch and Dr. C. Curfs for assistance with measurements on ID31.

REFERENCES

(1) Zhu, W. J.; Hor, P. H. *J. Solid State Chem.* **1997**, *130*, 319.
(2) Zhu, W. J.; Hor, P. H.; Jacobson, A. J.; Crisci, G.; Albright, T. A.; Wang, S.-H.; Vogt, T. *J. Am. Chem. Soc.* **1997**, *119*, 12398.

(3) Otzschi, K.; Ogino, H.; Shimoyama, J.; Kishio, K. *J. Low Temp. Phys.* **1999**, *117*, 729.
(4) Vajenine, G. V.; Hoffmann, R. *Inorg. Chem.* **1996**, *35*, 451.
(5) Ueda, K.; Hirose, S.; Kawazoe, H.; Hosono, H. *Chem. Mater.* **2001**, *13*, 1880.
(6) Gál, Z. A.; Rutt, O. J.; Smura, C. F.; Overton, T. P.; Barrier, N.; Clarke, S. J.; Hadermann, J. *J. Am. Chem. Soc.* **2006**, *128*, 8530.
(7) Mayer, J. M.; Schneemeyer, L. F.; Siegrist, T.; Waszczak, J. V.; Van Dover, B. *Angew. Chem., Int. Ed. Engl.* **1992**, *31*, 1645.
(8) Wang, C; Tan, M.; Feng, C; Ma, Z.; Jiang, S; Xu, Z.; Cao, G.; Matsubayashi, K.; Uwatoko, Y. *J. Am. Chem. Soc.* **2010**, *132*, 7069.
(9) Fuwa, Y.; Wakeshima, M.; Hinatsu, Y. *Solid State Commun.* **2010**, *150*, 1698.
(10) Matoba, M.; Takeuchi, T.; Okada, S.; Kamihara, Y.; Itoh, M.; Ohoyama, K.; Yamaguchi, Y. *Physica B* **2002**, *312*−*3*, 630.
(11) Okada, S.; Matoba, M.; Yoshida, H.; Ohoyama, K.; Yamaguchi, Y. *J. Phys. Chem. Solids* **2002**, *63*, 983.
(12) Okada, S.; Terasaki, I.; Ooyama, H.; Matoba, M. *J. Appl. Phys.* **2004**, *95*, 6816.
(13) Okada, S.; Matoba, M.; Fukumoto, S.; Soyano, S.; Kamihara, Y.; Takeuchi, T.; Yoshida, H.; Ohoyama, K.; Yamaguchi, Y. *J. Appl. Phys.* **2002**, *91*, 8861.
(14) Larson, A.; von Dreele, R. B. *The General Structure Analysis System*; Los Alamos National Laboratory: Los Alamos, NM, 1985.
(15) Prince, E., Ed. *International Tables for Crystallography, Volume C: Mathematical, physical and chemical tables*; International Union of Crystallography; Wiley: West Sussex, UK, 2004.
(16) Otwinowski, Z.; Minor, W. In *Methods in Enzymology, Macromolecular Crystallography, Part A*; Carter, C. W., Jr., Sweets, R. M., Eds.; Academic Press: New York, 1997; Vol.276.
(17) Farrugia, L. J. *J. Appl. Crystallogr.* **1999**, *32*, 837.
(18) Sheldrick, G. M. *SHELX97*, Programs for Crystal Structure Analysis, Release 97-2; University of Göttingen: Göttingen, Germany, 1997.
(19) Spek, A. L. *Acta Crystallogr. A* **1990**, *46*, C34.
(20) Blöchl, P. E. *Phys. Rev. B* **1994**, *50*, 17953.
(21) Hohenberg, P.; Kohn, W. *Phys. Rev.* **1964**, *136*, 864.
(22) Kohn, W.; Sham, L. J. *Phys. Rev.* **1965**, *140*, 1133.
(23) Kresse, G.; Furthmüller, J. *Comput. Mater. Sci.* **1996**, *6*, 15.
(24) Kresse, G.; Joubert, D. *Phys. Rev. B* **1999**, *59*, 1758.
(25) Perdew, J. P.; Burke, K.; Ernzerhof, M. *Phys. Rev. Lett.* **1996**, *77*, 3865.
(26) Perdew, J. P.; Burke, K.; Ernzerhof, M. *Phys. Rev. Lett.* **1997**, *78*, 1396.
(27) Dudarev, S. L.; Botton, G. A.; Savrasov, S. Y.; Humphreys, C. J.; Sutton, A. P. *Phys. Rev. B* **1998**, *57*, 1505.
(28) Smura C. F. D.Phil. Thesis, University of Oxford, 2008.
(29) Pitcher, M. J.; Smura, C. F.; Clarke, S. J. *Inorg. Chem.* **2009**, *48*, 9054.
(30) Palazzi, M. *C.R. Hebd. Seances Acad. Sci., Ser. C, Sci. Chim.* **1981**, *292*, 7899.
(31) Berger, R. *J. Less-Common Met.* **1989**, *147*, 141.
(32) Brown, I. D.; Altermatt, D. *Acta Crystallogr. B* **1985**, *41*, 244.
(33) Brown, I. D. , http://www.ccp14.ac.uk/ccp/web-mirrors/i_d_brown/bond_valence_param/, 2006.
(34) Lee, C. H.; Iyo, A.; Eisaki, H.; Kito, H.; Fernandez-Diaz, M. T.; Ito, T.; Kihou, K.; Matsuhata, H.; Braden, M.; Yamada, K. *J. Phys. Soc. Jpn.* **2008**, *77*, 083704.
(35) Yamada, K.; Matsuda, M.; Endoh, Y.; Keimer, B.; Birgeneau, R. J.; Onodera, S.; Mizusaki, J.; Matsuura, T.; Shirane, G. *Phys. Rev. B* **1989**, *39*, 2336.
(36) Figgis, B. N.; Hinchman, M. A. *Ligand Field Theory and its Applications*; Wiley-VCH: New York, 2000.
(37) Knee, C. S.; Weller, M. T. *Phys. Rev. B* **2004**, *70*, 144406.
(38) Jauch, W.; Reehuis, M.; Bleif, H. J.; Kubanek, F.; Pattison, P. *Phys. Rev. B* **2001**, *64*, 052102.
(39) Jauch, W.; Reehuis, M. *Phys. Rev. B* **2002**, *65*, 125111.
(40) Hubbard, J.; Marshall, W. *Proc. Phys. Soc. (London)* **1965**, *86*, 561.
(41) Hansteen, O. H.; Fjellvåg, H.; Hauback, B. C. *J. Solid State Chem.* **1998**, *141*, 41.
(42) Hansteen, O. H.; Fjellvåg, H.; Hauback, B. C. *J. Mater. Chem.* **1998**, *8*, 2089.
(43) Ceulemans, A.; Dendooven, M.; Vanquickenborne, L. G. *Inorg. Chem.* **1985**, *24*, 1159.
(44) Demazeau, G.; Buffat, B.; Pouchard, M.; Hagenmuller, P. *J. Solid State Chem.* **1984**, *54*, 389.
(45) Shannon, R. D. *Acta Crystallogr. A* **1976**, *32*, 751.
(46) Xiang, H. J.; Wei, S.-H.; Whangbo, M.-H. *Phys. Rev. Lett.* **2008**, *100*, 167207.
(47) Goodenough, J. B. *Magnetism and the Chemical Bond*; John Wiley & Sons: New York, 1963.
(48) Wright, J. P.; Attfield, J. P.; Radaelli, P. G. *Phys. Rev. B* **2002**, *66*, 214422.